Diode-Pumped Regenerative Amplifier for the NIF Laser System

J. K. Crane
M. Martinez
R. J. Beach
S. Mitchell
F. Penko
D. Browning
R. Wilcox

Introduction

The National Ignition Facility (NIF) laser pulse is born in the Master Oscillator Room (MOR) at very low energy (up to 1-nJ output). The energy increases as the laser pulse passes through the regenerative amplifier (up to 10-mJ output) and the 4-pass amplifier (up to 22-J output). Finally, in the full-aperture optics, up to 10 kJ of 351-nm light is reached on target.

To achieve ignition, the laser energy on target must be in the form of specifically tailored, high-fidelity temporal shape with a precise frequency spectrum. The optical pulse generation (OPG) system, or front end of the NIF laser system, consists of the MOR and the preamplifier modules (PAMs). The MOR produces the initial laser pulse in a Q-switched, single-mode, fiber, ring-laser oscillator. This laser pulse, which is reproduced 960 times per second, is shaped, modulated, amplified, and multiplexed to feed pulses to the 48 individual PAMs using fiber and integrated optical components.

The first laser system in a NIF beamline is the PAM. The input to the PAM is a 1-nJ shaped pulse that is delivered via single-mode, polarization-preserving fiber. The output is a 22-J pulse that is spatially shaped to meet the requirements of the main laser amplifiers. Figure 1 is a block diagram of a PAM showing its five component subsystems, namely, fiber injection, diode-pumped regenerative amplifier, spatial beam shaping, smoothing by spectral dispersion (SSD), and the 4-pass amplifier. The five subsystems are housed in a modular, I-beam-supported structure that is about $4.3 \times 1.0 \times 0.7$ m in size and contains all of the power, control, and diagnostic systems to make each PAM a complete system.

The PAMs produce the largest optical gain of the entire NIF laser system, boosting 1-nJ pulses from the MOR to 22 J. The performance specifications for the PAM and its component laser systems were determined as a flowdown from the output performance specifications of the overall NIF laser system, which are based on target requirements for ignition.[1,2] These specifications, listed in Table 1, include performance descriptions for both the regenerative and 4-pass amplifiers that are derived from the overall requirements of a PAM. We are allowed some flexibility to adjust the internal PAM parameters to produce the optimum design.

This article describes the current baseline diode-pumped regenerative amplifier and the results of a comprehensive series of measurements of its performance. In conjunction with these measurements, we have developed models allowing us to evaluate improvements to the baseline that will provide an additional margin to increase the performance of the entire preamplifier system.

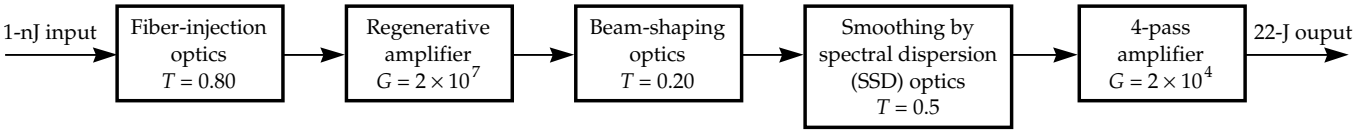

FIGURE 1. Block diagram showing the major subsystems within the NIF preamplifier modules (PAMs). *G* is gain; *T* is transmission loss.
(70-00-0298-0159pb01)

TABLE 1. PAM output specifications based on flowdown from the NIF laser system and target requirements.

	Parameter	Value
1.	Minimum PAM shaped energy	14.5 J
2.	Design energy*	22 J
3.	Peak power*	8.8 GW
4.	4-pass amplifier injection energy	1.0 mJ
5.	Regenerative amplifier output energy	10 mJ
6.	Pulse duration	21 ns
7.	Square-pulse distortion (regen)	1.2
8.	Square-pulse distortion (4-pass amplifier)	2.3
9.	Temporal contrast at PAM input	275:1
10.	Temporal contrast at PAM output	100:1
11.	Spatial profile	2:1
12.	Prepulse contrast	10^5–10^6
13.	Near-field spatial contrast	< 5%
14.	RMS energy fluctuation	<0.03

*Energy and power in a flat-top beam with a 90% fill factor

Description of the Regenerative Amplifier

In large, complex, solid-state laser systems, a regenerative amplifier (or regen) is often used to boost the output energy of the laser oscillator to a level that is suitable for injection into the larger power amplifiers. In this way, a regen is analgous to a high-fidelity preamplifier used in conventional radio frequency (rf) systems, such as stereos. A laser regen is an optical cavity with gain into which a low-energy laser pulse is injected, amplified by several orders of magnitude, then switched out of the cavity. For example, if the net gain per round trip in the cavity G_{net} is 3.0, and the pulse is allowed to circulate for $k = 15$ round trips, then the total unsaturated gain of the regen is

$$G_{total} = (G_{net})^k = (3.0)^{15} = 1.4 \times 10^7 . \quad (1)$$

The total gain is ultimately limited by the amount of stored energy that can be extracted from the amplifier. If a substantial amount of the stored energy in the amplifier is removed, then G_{net} drops below 1.0 (G_{net} is the product of the gain in the amplifier G and the transmission losses in a single round trip T, such that $G_{net} = GT$), and G_{total} decreases as a function of round trip because the amplifier gain is saturated.

The MOR generates pulses up to 21 ns long with a particular temporal shape determined by the target requirements. This specially shaped pulse must be amplified with a high degree of fidelity to ensure that the desired shape is preserved to the end of the laser chain. Based on its method of operation, the regen cavity must be long enough to contain an entire 21-ns pulse without a temporal overlap between the beginning and end of the pulse. Two types of regen cavities are found in the Laser Programs: space ring cavities[3,4] and linear cavities.[5] Each type has certain advantages over the other.

In a ring cavity, the pulse circulates in one direction in a closed path. The perimeter of the ring must be longer than the pulse length; that is, perimeter $> c(T_{pulse} + T_{switch})$, where c is the speed of light. Some additional length, cT_{switch}, provides time for a Pockels cell to switch the polarization of the light pulse and trap it in the cavity. This additional switching time is 3–5 ns, depending on the rise time of the Pockels cell. The linear cavity can be approximately half as long as the perimeter of the ring cavity because the pulse can partially overlap itself in the cavity as long as the front and tail ends of the pulse do not overlap in the Pockels cell during switching.

Figure 2 shows the current prototype regen. The cavity is a folded linear design with a diode-pumped rod amplifier at either end. A pulse propagating in the cavity double-passes through each rod amplifier. A rod amplifier has a single-pass gain of 1.5; thus the gain per round trip is $(1.5)^4 T$, where T is the round trip transmission of the cavity. A 2.0-m focal length lens in the center gives the cavity a stability value of $g^2 = 0.02$, and an adjustable iris is used to limit the spatial modes to one. In the current design, the cavity has a round trip time of 30 ns, allowing us to cleanly switch a pulse as long as 24 ns into and out of the cavity.[6]

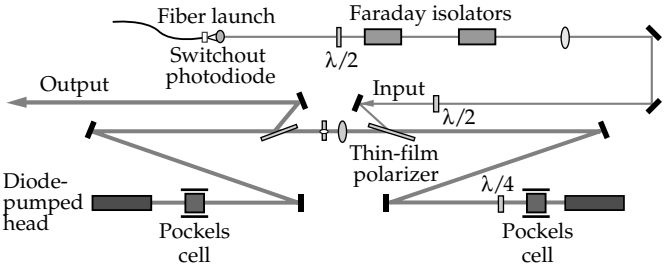

FIGURE 2. Baseline regenerative amplifier with optics for seeding the cavity from a single-mode fiber. (70-00-0298-0160pb01)

The seed pulse from the MOR is introduced into the cavity by reflection from a thin-film polarizer. A two-lens telescope, which is part of the optics for seeding the regen, is designed to match the output mode from the fiber to the eigenmode of the cavity. In the first cavity round trip [Figure 3(a)], both Pockels cells are off, and the s-polarized pulse is converted to p polarization upon double passing a quarter-wave plate. After the tail of the pulse passes [Figure 3(b)], the Q-switch Pockels cell fires, trapping the p-polarized pulse in the cavity. The quarter-wave plate and Pockels cell produce equal retardation, so the pulse is trapped in the cavity for the desired number of round trips, whereupon the cavity-dump Pockels cell fires, and the amplified pulse is ejected [Figure 3(c)].

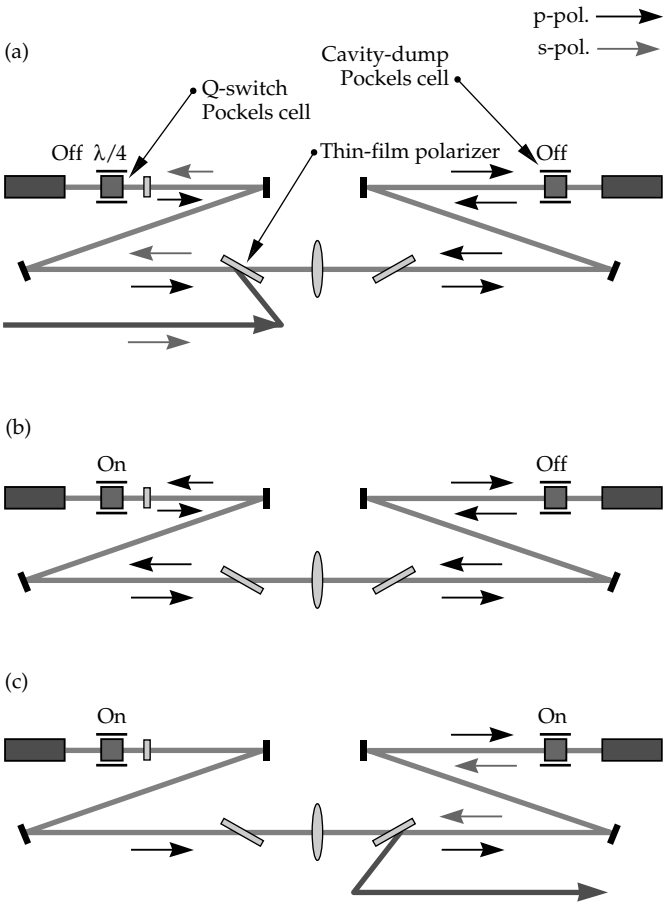

FIGURE 3. Polarization states in the regenerative amplifier. (a) When injecting the seed, both polarizers are off. (b) When Q-switching or trapping the pulse in the cavity, the Q-switch Pockels cell is on. (c) During switchout of the amplified pulse, the cavity-dump Pockels cell is turned on. Gray arrows represent s-polarization; black arrows represent p-polarization. (70-00-0298-0161pb01)

Diode-Pumped Rod Amplifiers

The diode-pumped rod amplifiers used in the regen are similar in design to several others developed by LLNL's Solid-State Laser Group and are described in detail in several publications.[6,7] Figure 4 shows a picture of the head with labels for each of the key components. In the currently operating regen, the pump light in each head is produced by a diode array, consisting of forty-eight 100-W diode bars stacked in an array with 1-mm spacing between bars. Spectra Diode Labs (SDL) makes the diode bars. The laser light from each bar is conditioned by a cylindrical microlens to produce a far-field cone with angular dimensions of 80 × 240 mrad. The diode light is collected by a tapered lens duct that funnels the pump light into the end of the amplifier rod. The rod is 5 mm in diameter by 50 mm long and made of Nd-doped phosphate glass (LG760 or APG1). The end of the rod adjacent to the lens duct is coated to efficiently pass the pump light but reflect the 1053-nm wavelength light. This surface is the back mirror of the regen cavity. The Nd doping of the rod is specified to provide a single-pass absorptivity of 1.5 at the absorption peak near 800 nm. The diode array, lens duct, and rod are packaged as shown in the Figure 4. The rod is mounted with a surrounding plenum that allows for dry nitrogen cooling to reduce temperature gradients. Nitrogen exhausted from the rod plenum flows over a fin-shaped structure that thermally contacts the diode array and provides some cooling to the diodes themselves.

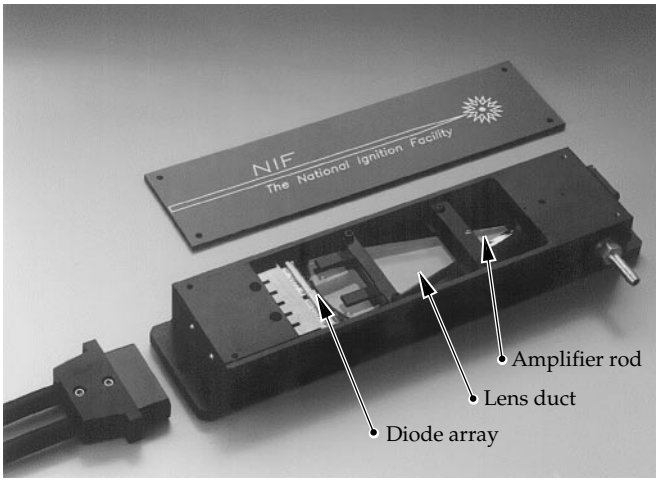

FIGURE 4. A 48-bar diode array with microlenses end pumps a 5- × 50-mm rod. The lens duct focuses light from the array into the rod. (70-00-0298-0162pb01)

Performance Measurements

Diode Pumping

The diode arrays were initially characterized before being assembled into the diode-pumped rod amplifier packages. Light energy out of the diodes, after the microlensing and at the output of the lens duct, was measured as a function of diode-driver current using an integrating sphere. Figure 5 shows the results of measurements for one of the two diode heads used in the current regen. The data show that the array has a slope of 59.2 W/A; at 100 A of current, the optical pump power at the input to the laser rod is 3.6 kW. The efficiency for collecting and transporting diode-pump light to the end of the rod is 86%. For a 350-μs-long square pulse, the optical pump energy at the rods is 1.12 and 1.26 J for head one and two, respectively.

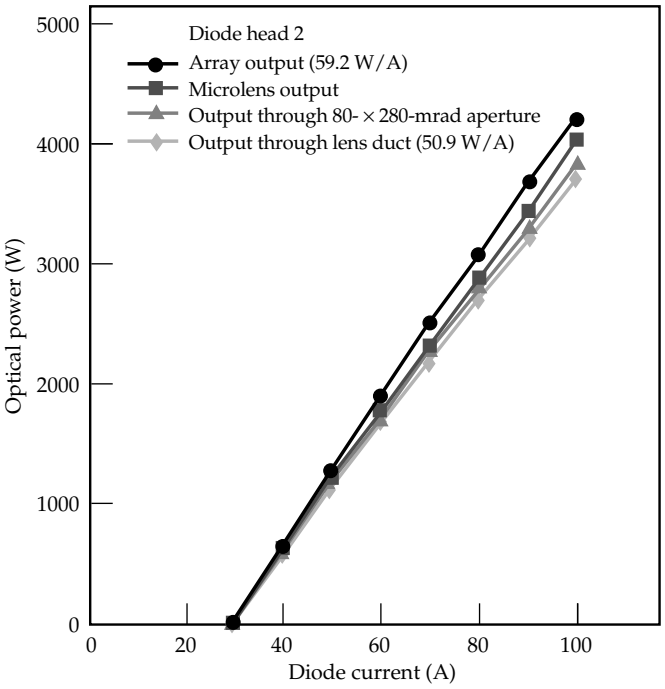

FIGURE 5. Measured optical power from one of the two diode arrays in the regen amplifier heads. (70-00-0298-0163pb01)

As part of the initial characterization of the diode arrays, we measured their output spectrum using a quarter-meter spectrometer with a camera at the output. Figure 6 shows the output emission spectrum from the diodes along with the absorption spectrum of the laser glass, LG760. Each diode package for a rod amplifier consists of two arrays that are mounted side-by-side on a single heat sink. The single Gaussian-shaped emission indicates that the separate arrays closely overlap in wavelength.

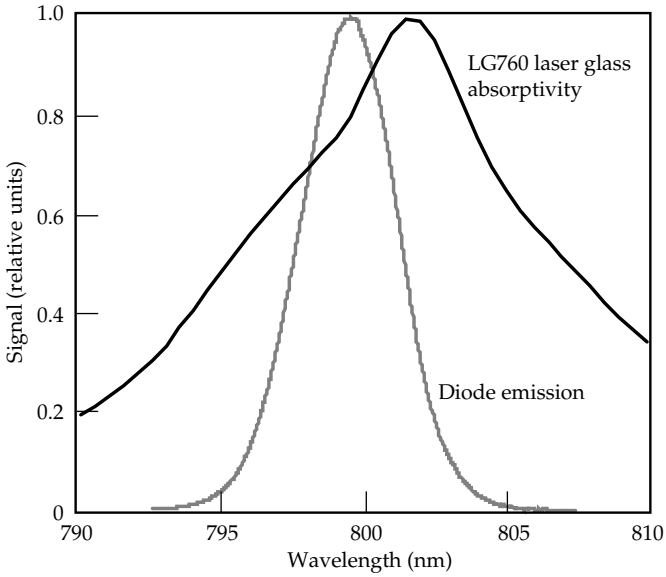

FIGURE 6. Normalized emission spectrum from diode head number 1 (DH1) (gray curve) and LG760 absorptivity (black curve). (70-00-0298-0164pb01)

From the data on diode emission and glass absorption, we can determine the absorption efficiency of diode pumping. We define a diode-emission spectral power density $\rho_{diode}(\lambda)$ such that the output power of the diode array is

$$P_{diode} = \int_{-\infty}^{\infty} \rho_{diode}(\lambda) d\lambda \ . \quad (2)$$

The transmission of the Nd-doped glass is given by

$$T(\lambda) = \exp[-\alpha(\lambda) 2d] \ , \quad (3)$$

where $\alpha(\lambda)$ is the absorptivity per unit length of laser medium, and d is the rod length. Figure 7 shows the normalized diode-emission power density $\rho_{diode}(\lambda)$ and glass transmission $T(\lambda)$ as well as the fraction of the diode emission that is absorbed and transmitted after two passes through the rod. The ratio of power absorbed to diode power emitted gives the absorption efficiency η_{abs} as follows

$$\eta_{abs} = 1 - \frac{\int_{-\infty}^{\infty} \rho_{diode}(\lambda)\ \exp[-\alpha(\lambda)2d]d\lambda}{\int_{-\infty}^{\infty} \rho_{diode}(\lambda)d\lambda} \quad . \qquad (4)$$

For the data shown in Figure 7, the absorption efficiency is 90%. This value could be increased by shifting the wavelength of the diodes to better overlap the peak of the absorption curve, or by increasing Nd^{3+} doping to provide increased absorption.

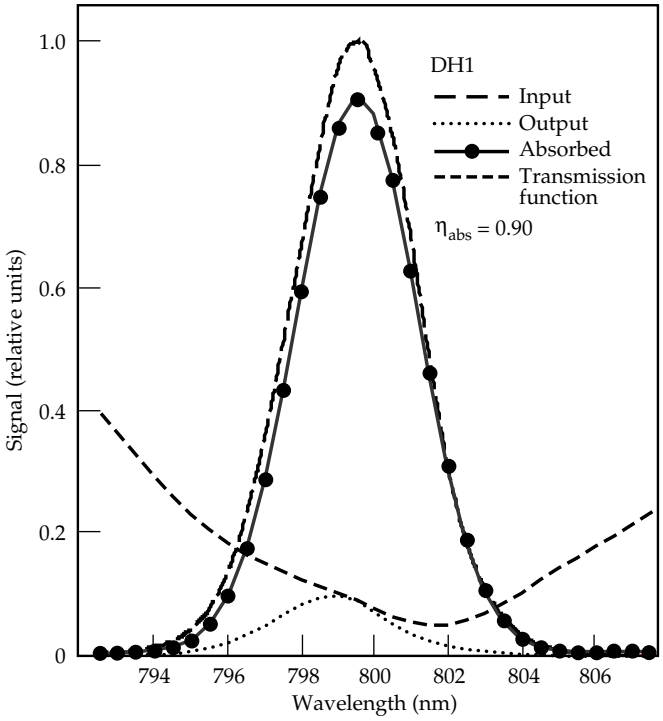

FIGURE 7. Normalized emission at rod input, output emission after double passing through rod, amount absorbed, and transmission function of LG760 glass. (70-00-0298-0165pb01)

An important step toward understanding the energetics of the regen is to characterize the gain in the diode-pumped rod amplifiers. We measured double-pass gain through the rod amplifier using a small probe laser, as shown in Figure 8. (Recall that the rod amplifier is end pumped, so there is only access at one end of the rod for measurements.) We can vary the arrangement shown Figure 8 to probe either a small volume in the center of the rod or to measure gain over the entire rod diameter. For probing a small volume in the center of the rod, we use photodiodes as reference and signal detectors. The double-pass gain is the ratio of the detector signals:

$$G^2(\lambda,t) = S_{sig}(\lambda,t)/S_{ref} \ . \qquad (5)$$

The square-root of the detector signal ratio yields the single-pass gain. The wavelength λ and time-dependence are important to note. We used a narrow-band, Nd-doped yttrium lithium fluoride (Nd:YLF) probe laser whose wavelength is centered on the regen gain spectrum; alternatively, we can use the MOR pulse to probe the regen gain. We measured the gain at the end of the 350-μs pump pulse where it is at a maximum value and, consequently, when we Q-switch the regen.

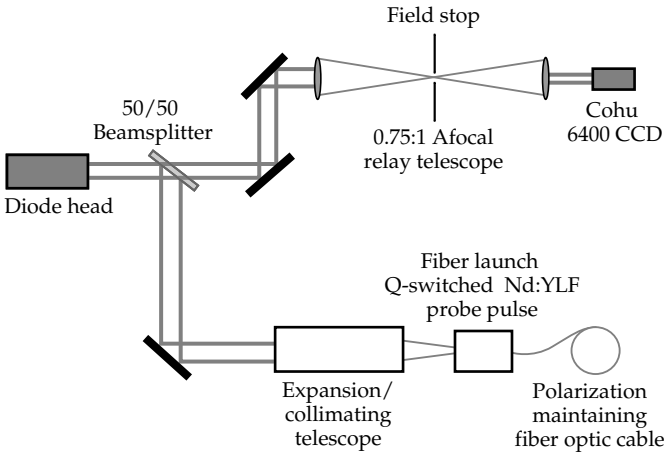

FIGURE 8. Optical layout for measuring spatial gain profiles. (70-00-0298-0166pb01)

Figure 9(a) shows the measured, single-pass gain G_1 as a function of diode-driver current using the YLF laser as a probe. In Figure 9(b), we converted the gain data to stored energy using the relation $E_{stored} = AJ_{sat}\ln(G)$ and plotted stored energy vs diode current, as shown. The solid line plotted with the data represents a simple model for stored energy vs diode pump power

$$P_{pump} = \frac{E_{stored}}{\eta_{ext}\eta_{del}\eta_{abs}\ QD\left(1 - e^{\tau_P/\tau_0}\right)}\ \frac{1}{\tau_0} \quad , \qquad (6)$$

where η_{ext}, η_{del}, and η_{abs} are the efficiencies for producing diode emission, delivering the emission to the rod, and absorbing the energy into the upper laser level of the glass, respectively; *QD* is the quantum defect of the upper laser transition; τ_p is the pump period; and τ_0 is the spontaneous emission lifetime of the upper laser level. Values for the constants in Eq. (6) are:

$\eta_{del} = 0.75$
$\eta_{ext} = 0.83$
$\eta_{abs} = 0.90$
$QD = 0.76$
$\tau_0 = 320$ μs and
$\tau_p = 350$ μs.

The data depart from the model at about 80-A diode current, or $G = 1.48$ to 1.50. Several different explanations could account for the rolloff in gain. For example, the diode-emission frequency could be changing frequencies (chirping) away from the absorption line center of the glass at the end of the current pulse. If the amount of chirp increases with increasing diode current, then the absorption efficiency η_{abs} would decrease, causing the stored energy described by Eq. (6) to roll over, as shown in Figure 9(b). Another contributor could be amplified spontaneous emission that is quenching the stored energy in the upper laser level, causing the gain to roll over with increasing current as shown. The amplifier rods have highly polished barrels to permit total internal reflection (TIR) of pump light and help homogenize the spatial gain distribution. Unfortunately, the polished sides can also support long-pathlength propagation at the laser wavelength, such as whisper modes, that effectively clamp the gain and reduce pump efficiency.

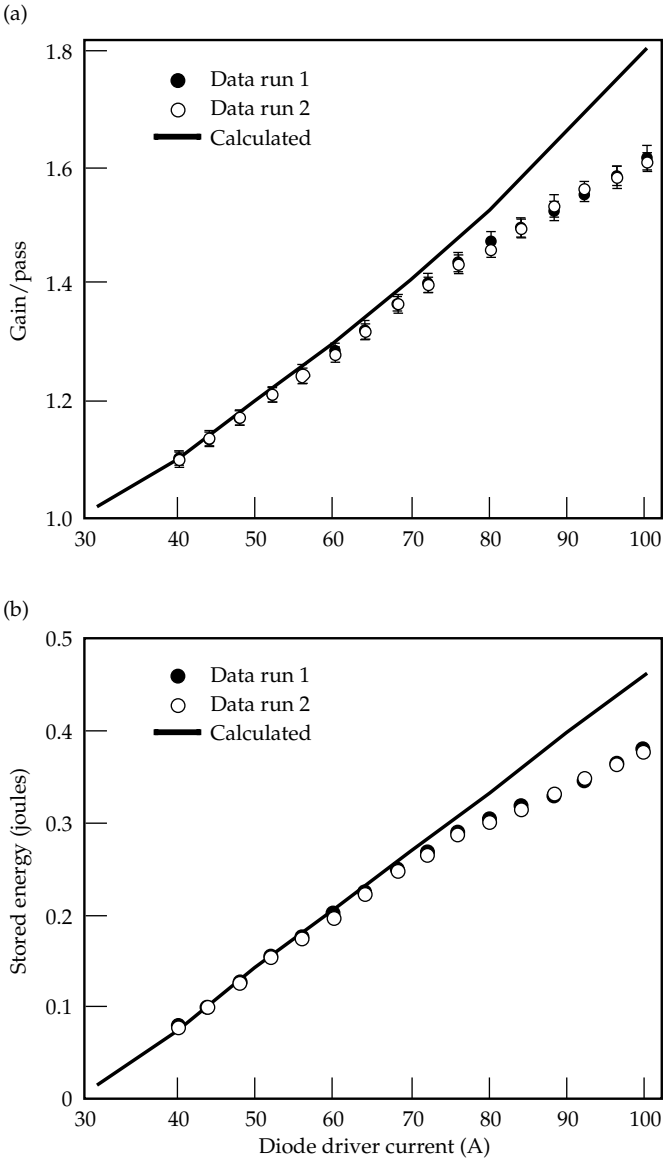

FIGURE 9. (a) Gain per pass and (b) stored energy for diode-pumped rod amplifiers with LG760 glass. The solid line is the model prediction. (70-00-0298-0167pb01)

Regen Gain and Loss Measurements

As part of our comprehensive characterization of the laser system, we made a series of careful measurements of gain, loss, output energy, and power from our baseline regen. In conjunction with these measurements, we developed a model that accurately reproduces the measured results and that can now be used to help optimize the current design.

Figure 10 shows the layout of the regen with its seeding optics and several diagnostics used in the measurements. We recorded the temporal pulse shapes at the input and output to the regen, and by looking at the pulse buildup in the cavity immediately before the output thin-film polarizer. We measured the output energy from the regen with Molectron calorimeters (the choice of calorimeter depends on the energy range being measured). The measured energy value at the calorimeter is divided by the value of the measured optical transmission between the output of the regen and the location of the calorimeter to give a value that is equivalent to the regen output energy. For a single regen shot, we recorded the three photodetector signals and the calorimeter reading. We converted the temporal signals $S(t)$ from the output and cavity buildup detectors to power P(t) vs time by dividing the integrated detector signal by the measured energy E, according to

$$P(t) = \frac{ES(t)}{\int S(t)dt} \quad . \tag{7}$$

The input calorimeter was calibrated separately by placing a J3S calorimeter head directly after the input thin-film polarizer. We then compared the integrated temporal signal from the input photodetector to the calorimeter value to obtain a calibration factor to convert the temporal signal to power. In this way, we can record on any shot the power at the regen input and output, and the power buildup inside the cavity for each pass.

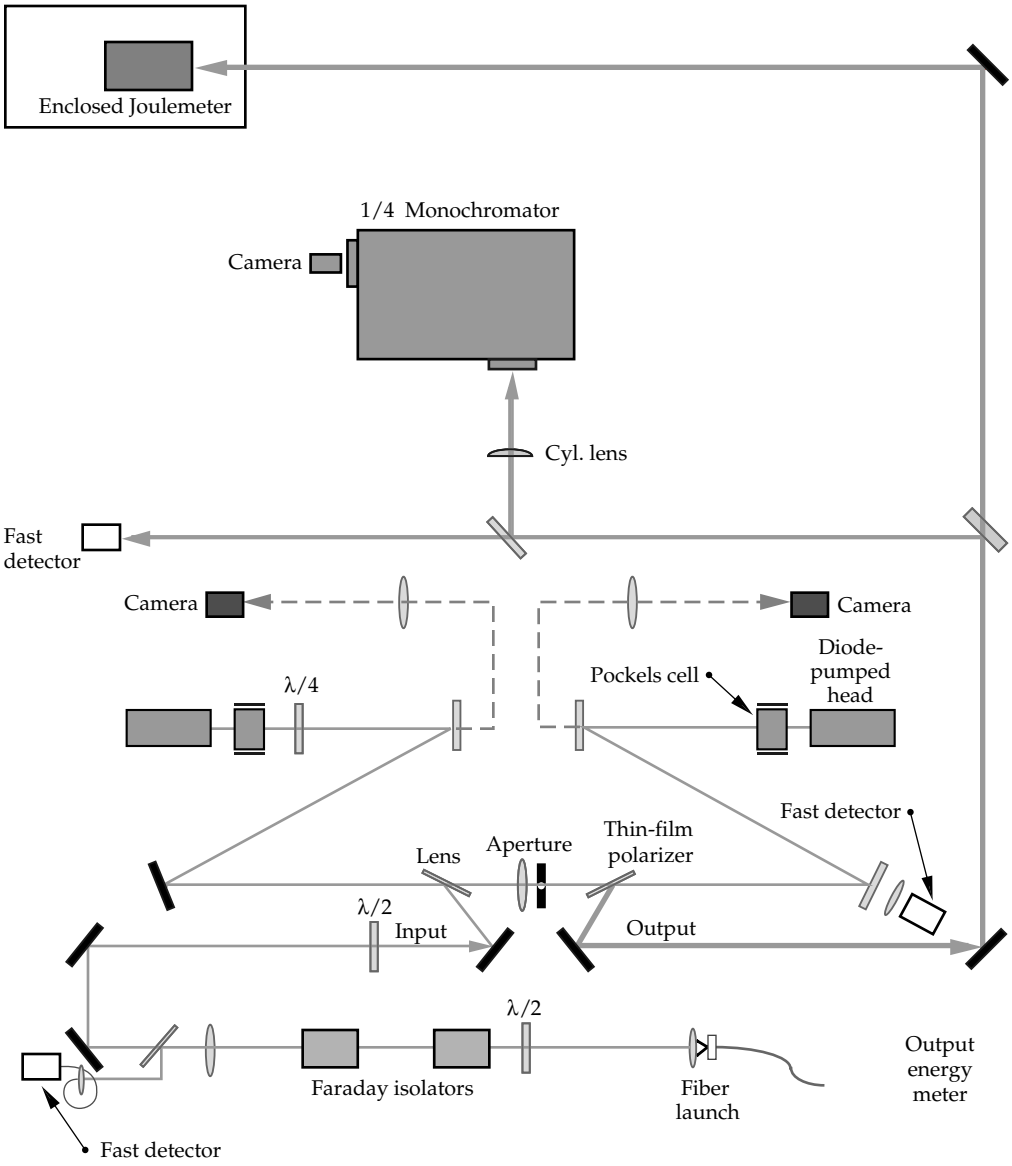

FIGURE 10. Setup for measuring regen energetics. Diagnostics include fast photodiodes at the input and output, and looking in the cavity for measuring temporal pulse shapes; cameras to measure the mode size; a small monochromator for measuring spectra; and input (not shown) and output calorimeters for measuring energy. (70-00-0298-0168pb01)

In addition to the power and energy from the regen, we measured the spectral overlap between the seed from the MOR and the gain spectrum of the regen. We also measured and recorded the spatial extent of the laser mode on each rod by imaging the mode at the rod input onto a calibrated charged-coupled device (CCD) camera that is part of a Big Sky beam-profiling system. The spatial information allows us to convert the measured power and energy for each round trip into irradiance $I(r,t)$ in the gain medium according to

$$I(r,\theta,t) = \frac{P(t)R(r)\Theta(\theta)}{\int R(r)\Theta(\theta)rdrd\theta} \rightarrow \frac{P(t)R(r)}{2\pi\int R(r)rdr} \quad , \qquad (8)$$

where $R(r)$ is the radial dependence, and the azimuthal dependence $\Theta(\theta)$ is assumed to be constant for a TEM_{00} mode.

To complete our suite of energetics measurements for the regen, we measured the cold transmission of the laser pulse for one round trip in the cavity. We made this measurement using three different techniques that yield similar answers. The easiest way to measure cavity transmission is to measure the relative intensity of a continuous wave (cw) beam that is sent into the cavity through the same seed optics so that it is mode-matched to the cavity. We used this technique as a diagnostic to look for problems, such as bad coatings, clipping in the cavity, or stress-induced birefringence.

The second technique for measuring cavity transmission is to switch in a seed pulse with the rod amplifiers turned off, switch it out after successive numbers of round trips, and measure the "ringdown" or attenuation of the pulse per round trip. The ringdown technique, which is dynamic and includes switching losses from the Pockels cells, indicates seeding of multiple roundtrips, which is undesirable. Figure 11 shows the data for a ringdown measurement as well as the value for the static transmission measured with a cw beam.

The third technique is to measure the output of the regen after the first few round trips with the amplifiers

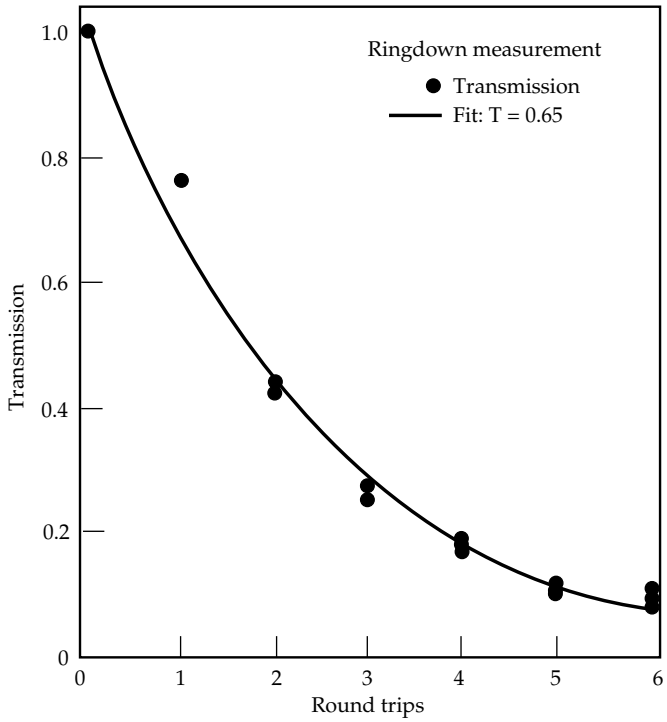

FIGURE 11. Cold-cavity ringdown measurement of regenerative amplifier round-trip transmission. (70-00-0298-0169pb01)

on. We repeated the measurement for different values of pump-diode current, and measured a net gain per round trip, as shown in Figure 12. Using the values of gain per pass measured for the rod amplifiers (see Figure 9), we obtained a value of round-trip transmission that includes any additional losses from the energized rod amplifiers, where $T = G_{net}/(G_1^2 G_2^2)$. These three different techniques for measuring the round-trip cavity transmission in the current design yield values that range between T = 0.59–0.65. We are working on alternative cavity designs that will increase the value of cavity transmission by eliminating one Pockels cell and thin-film polarizer (TFP) and using the remaining TFP in reflection rather than transmission.

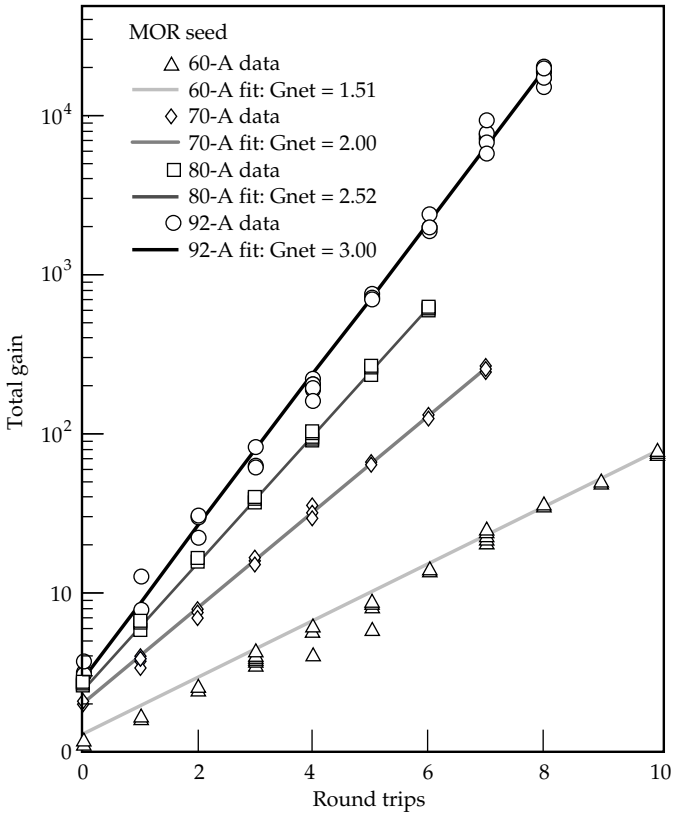

FIGURE 12. Small signal gain in the regen for different values of pump-diode current. (70-00-0298-0170pb01)

Saturated Gain Measurements

Description of the 2-D Model

We developed a time-dependent model to describe the gain $G(t)$ and circulating irradiance $I(t)$ in the regen. The current version is based on the time-dependent equation for gain[8]

$$G(r,t) = \frac{1}{1 - \left[1 - \frac{1}{G(r,0)}\right] \exp\left[\frac{-U(r,t)}{J_{sat}}\right]} \quad , \tag{9}$$

where J_{sat} is the saturation fluence of the laser transition, $G(r,0)$ is the initial gain as a function of radius in the rod, and

$$U(r,t) = \int_0^t I(r,t')dt' \quad . \tag{10}$$

The radial dependence of the cavity eigenmode is included to more accurately describe spatial saturation in the amplifier rod. If the mode is treated as an equivalent flat top with equal energy and peak irradiance, then the model predicts a much faster falloff of energy after full saturation. In the two-dimensional (2-D) model, we use the measured Gaussian cavity mode, providing a radial dependence to the gain saturation. However, because the regen is a seeded oscillator with a single-cavity spatial eigenmode, we renormalize the spatial dependence of the irradiance to this mode after each round trip.

The current regen has end-pumped, diode-pumped rod amplifiers at either end of the cavity; consequently, the laser pulse folds back on itself temporally in the gain medium. As a result of the pulse overlap, the trailing portion of the pulse is more strongly saturated than in the case of no overlap, as in a ring cavity, and square-pulse distortion (SPD) will be more severe.

The modeling and data analysis were both performed using a software package called IGOR developed by WaveMetrics, Inc., Lake Oswego, Oregon. The model inputs describing the regen energetics include the input pulse (power vs time), gain in each amplifier, mode size in each rod, round-trip cavity transmission, saturation fluence of the laser transition (we used the value of 3.99 J/cm^2 for LG760 from Ref. 9), and the number of round trips. The model calculates the time-dependent gain $G(r,t)$ and irradiance $I(r,t)$ on each pass using Eq. (9). From these two quantities, the model determines the power, energy, and square-pulse distortion at the regen output, the power and energy buildup in the cavity, and the spatial and temporal gain saturation in the amplifiers. We can then compare these model results with the data.

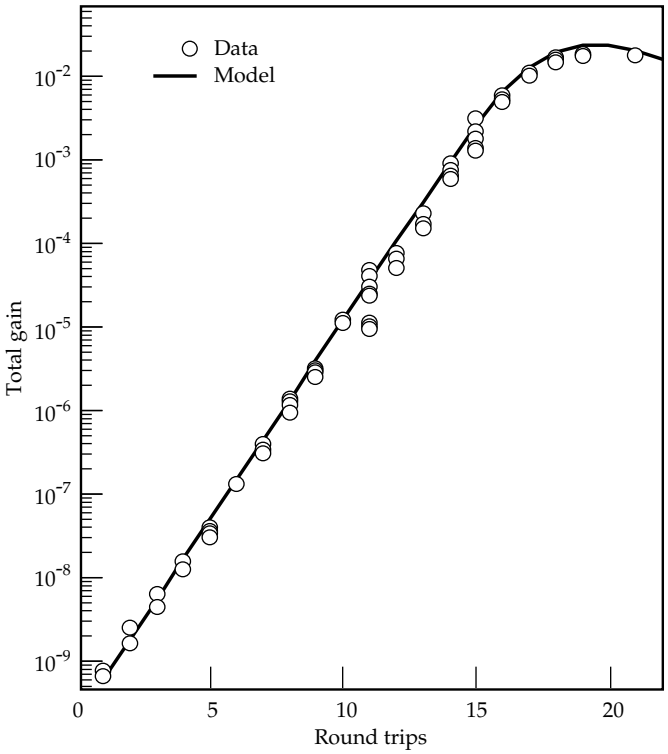

FIGURE 13. Comparison between 2-D Frantz–Nodvik model and data for regen output energy. Model parameters are $G_1 = G_2 = 1.50$; round-trip cavity transmission $T = 0.60$; beam waist $w_0 = 0.80$ cm, and input energy $E_{in} = 177$ pJ. (70-00-0298-0171pb01)

Comparisons of Model and Data

Figure 13 shows a measurement of output energy from the regen as a function of round trips for a fixed value of diode pump power. The measurement was made over the full dynamic range of the regen, that is, eight decades. Four different calorimeters were used to cover the full range. When we were close to the upper limit of one calorimeter, we repeated the measurement with a less sensitive calorimeter and used reference photodiodes as cross checks. The solid line in Figure 13 shows the model prediction for the input parameters given in the caption. The radial dependence of the mode in the rod must be included for the model to replicate the slow rolloff in the energy after the gain peak. The peak energy extracted is 22 mJ, corresponding to 63% of the stored energy in the mode volume of both amplifiers and consistent with the cavity transmission that falls between 59 and 65%.

Figure 14 shows model predictions of output power vs time for a pulse switched out of the cavity after 12 round trips. In Figure 14(a), we calculate an input square pulse that is equal in energy and peak power to the measured input pulse, and propagate that pulse using our model. This procedure facilitates the calculation of square-pulse distortion (SPD). With only 79 μJ extracted from the available 35 mJ, the gain saturation is negligible, and SPD = 1.003. Figure 14(b) compares the measured output pulse and the model output using the measured input pulse as the model input. The amplitude modulation on the real pulse appears at both regen input and output and arises from mode beating in the fiber master oscillator.

Figure 15 shows a 12.0-mJ output pulse switched out of the regen after 17 round trips. We repeated the comparison between the measured output pulse and a modeled square pulse, and the measured input pulse propagated through the model. We still find good agreement between the model pulses and the actual measured pulses, although they do not overlay exactly as in the lower-energy pulse in Figure 14. The output detector has a lower bandwidth than that of the input detector, so there may be some distortion of the sharper features. Comparing the square pulse output to the actual output pulse, we see that the break points at the peak of the pulse and in the dropoff portion of the pulse agree in amplitude, so the value of SPD = 1.54 is accurate.

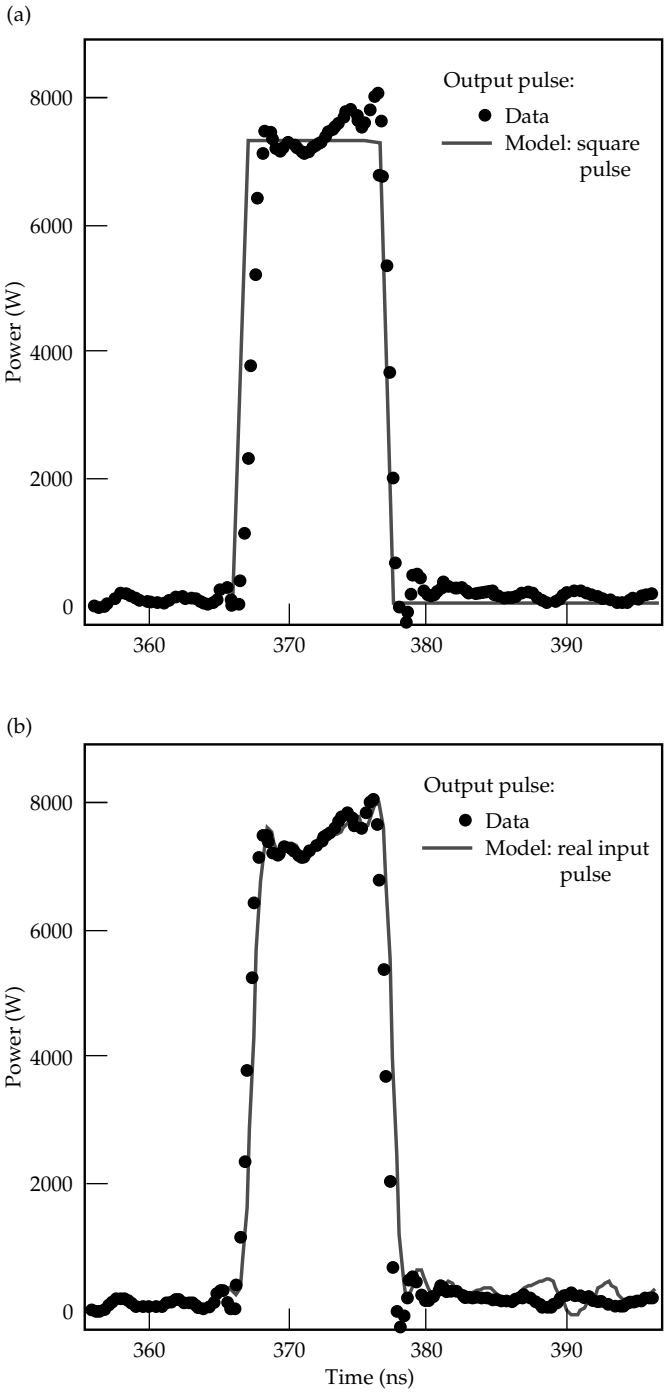

FIGURE 14. Model vs measured regen output pulse, where E_{in} = 147 pJ, E_{out} = 79 μJ, 12 round trips, G_1 = 1.495, G_2 = 1.50, cavity transmission T = 0.60, and SPD = 1.003. (70-00-0298-0172pb01)

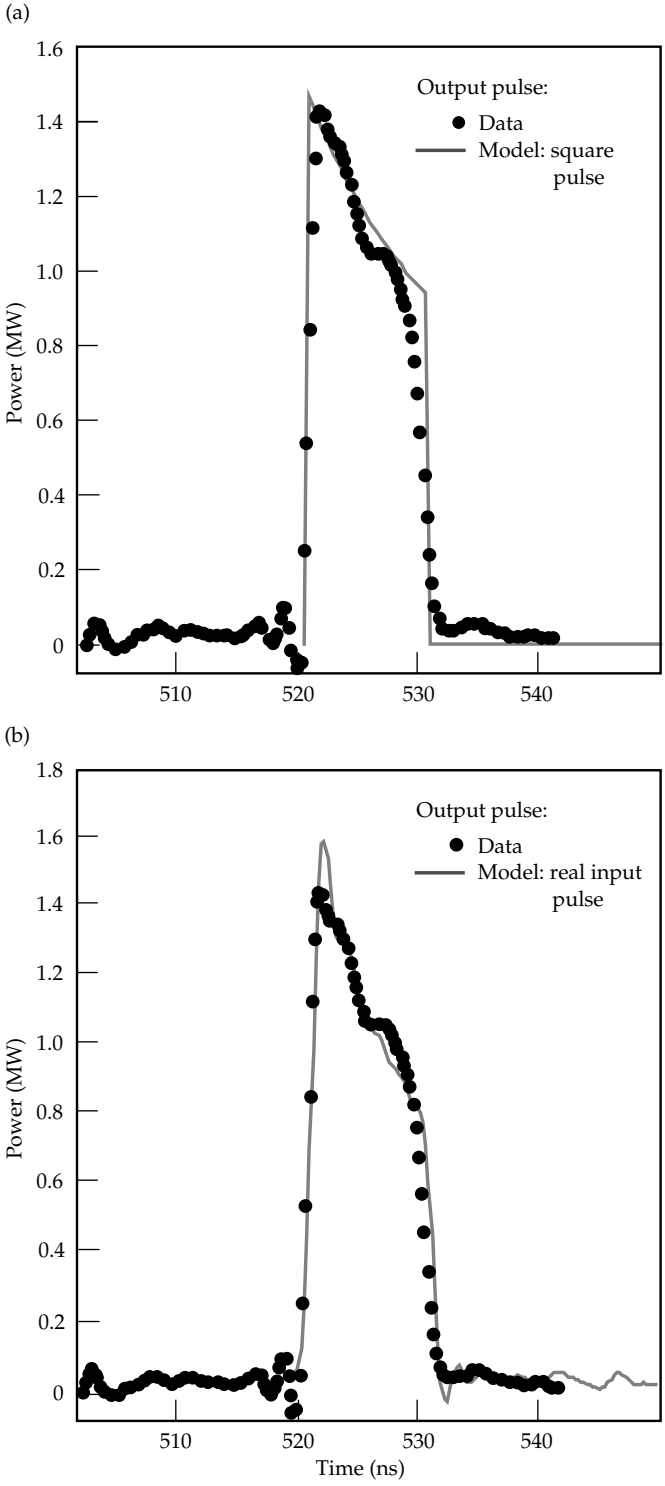

FIGURE 15. Comparison between model and data for a 12.0-mJ pulse. (a) Equivalent square pulse plus measured pulse. (b) Real pulse input to model compared with measured output pulse: SPD = 1.54. (70-00-0298-0173pb01)

Comparisons between the energy and power data from the regen and the model shown in Figs. 13 through 15 demonstrate very good agreement. Our goal was to develop a model that accurately predicts the output power, energy, and gain saturation of the NIF regenerative amplifier for a given set of inputs, and to use this model to examine ways to improve the performance of the regen. Features such as radial gain saturation and temporal pulse overlap in the amplifiers were added to the original, time-dependent saturation model

to accurately reproduce the slow rolloff in energy output after the peak, and to replicate the large amount of temporal pulse distortion observed in the data.

Signal-to-Noise Measurements

The ability to control the temporal pulse shape, hence pulse power of the laser system, resides in the OPG up to the output of the regen slicer. The remainder of the laser system consists of large amplifiers that can distort the pulse and add noise, but they cannot be used to affect controlled changes to the pulse shape. The noise added by the regen and MOR tend to set the upper acceptable limit for the entire laser system; thus, it is important that we measure and understand these sources of noise. The original specifications for the regen include a signal-to-noise ratio (S/N) of 10^4 for a 500-pJ input and a prepulse contrast between 10^5 and 10^6 (Refs. 3 and 4).

To determine the S/N at the output, we measured the noise power at the output photodiode with the input seed blocked and unblocked. This technique requires a detector that can accurately measure two signals that differ in amplitude by 4 to 5 orders of magnitude. We used a Hamamatsu vacuum photodiode and calibrated neutral-density filters to provide a known amount of attenuation. Figure 16 shows the output power of the regen with the input seed blocked and unblocked. An 18.6-mJ pulse is switched out after 18 round trips, and the peak power of the 10-ns pulse is 2.7 MW. When the seed is blocked, the output power drops to 160 W. The trapezoidal shape of this pulse reveals the switching window of the regen and is the shape of the noise pedestal atop which the amplified seed pulse rides. This measurement technique underrates the S/N value because the seeded regen is saturated, whereas the unseeded measurement is still in the small-signal regime. With fewer round trips, we cannot detect the regen output when the seed is blocked.

To determine the noise-equivalent power (NEP) at the input of the regen, we used our 2-D model. First, we constructed a square pulse of equivalent energy and peak power as the measured input pulse. We used this pulse as an input to the model and propagated it for the actual number of round trips, 18, that corresponds to the data. We adjusted the values of single-pass gain until we accurately reproduced the measured output pulse. A comparison between the measured and modeled output pulse is shown in Figure 16(b). Next, we constructed a trapezoidal-shaped input pulse to represent the noise pulse. We used the same values of gain per rod and transmission as required to reproduce the seeded output pulse, and adjusted the input energy of the noise pulse until we reproduced the measured output pulse shown in Figure 16(b). Figure 16(a) compares the model input pulses that were required to duplicate the measured output pulses using the model. From Figure 16(a), we obtained the energy and power S/N referenced to the input of the regen. Here, S/N (energy) = 1.29×10^4, S/N (power) = 1.75×10^4, and the NEP at the input of

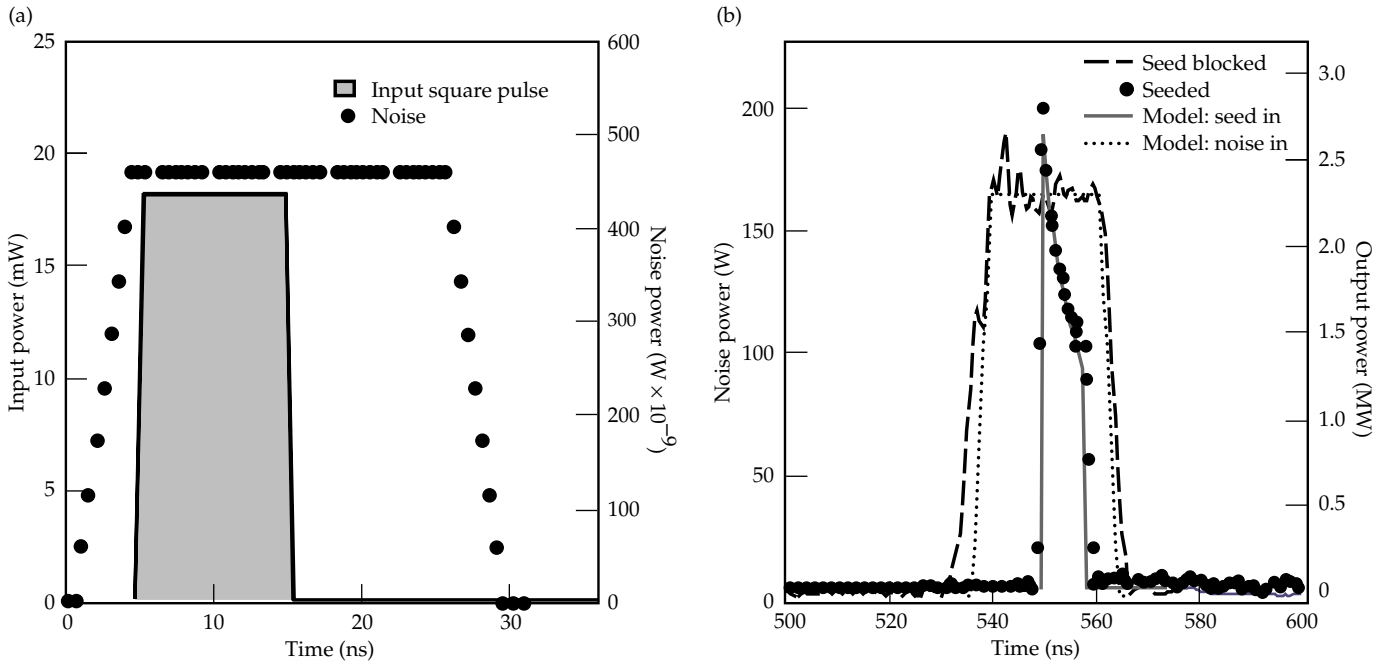

FIGURE 16. (a) Model input pulses consisted of a 181-pJ square pulse and 14-fJ noise pulse. (b) Comparison between measured output pulses and model results using the input pulses shown in (a). (70-00-0298-0174pb01)

the regen is 460 nW. As expected, the power S/N referenced to the input of the regen is larger than the ratio obtained by measuring the power ratio of the output pulses, where saturation must be considered.

To compare this measured noise value with the fundamental quantum limit, we seeded our regen model with a single spontaneous-emission photon per cavity mode over the full emission bandwidth of the laser transition in LG760. The noise energy E_{noise} is given by[10]

$$E_{noise} = \frac{h\nu}{2} \; N_{mode} = \frac{h\nu}{2} \Delta\nu_{SE} \left(\frac{2L}{c} \right) \quad , \tag{11}$$

where $h\nu$ is the photon energy, N_{mode} is the number of cavity modes, $\Delta\nu$ is the spontaneous emission bandwidth, L is the regen cavity length, and c is the speed of light. The spontaneous emission bandwidth $\Delta\nu_{SE}$ for LG760 corresponds to a FWHM of 20 nm. The number of noise photons is reduced by one-half in Eq. (11) because of the polarization selectivity of the cavity. To compare the quantum-limited noise energy with the measured value in Figure 16, we propagated the noise input spectrum, given by Eq. (11) for 18 round trips, using a Lorentzian-shaped gain spectrum for the amplifiers

$$g(\nu) = \frac{g(\nu_0)(\Delta\nu_{1/2})^2}{(\Delta\nu_{1/2})^2 + (\nu - \nu_0)^2} \quad , \tag{12}$$

where the peak centerline gain $g(\nu_0) = 4\ln G = 1.62$, and $\Delta\nu_{1/2} = \Delta\lambda_{1/2} c/\lambda^2$ is the FWHM of the exponential gain spectrum of LG760 (here, $\Delta\lambda_{1/2} = 20$ nm; that is, it is easier to think of bandwidth for broad spectral lines in terms of nm rather than Hz). After 18 round trips, the initially broad spectrum narrows to the 2.7-nm amplified noise spectrum shown in Figure 17. To determine the noise-equivalent energy (NEE) referred to the input, we divide the output energy by the total gain from 18 round trips, where $G_{total} = (G^4 T)^{18} = 4.8 \times 10^8$. The quantum-limited NEE, referenced to the input of the regen, is 2.28 fJ as shown in Figure 17. The quantum-limited NEP for the trapezoidal-shaped power pulse that is characteristic of the regen noise shown in Figure 17 is 84 nW.

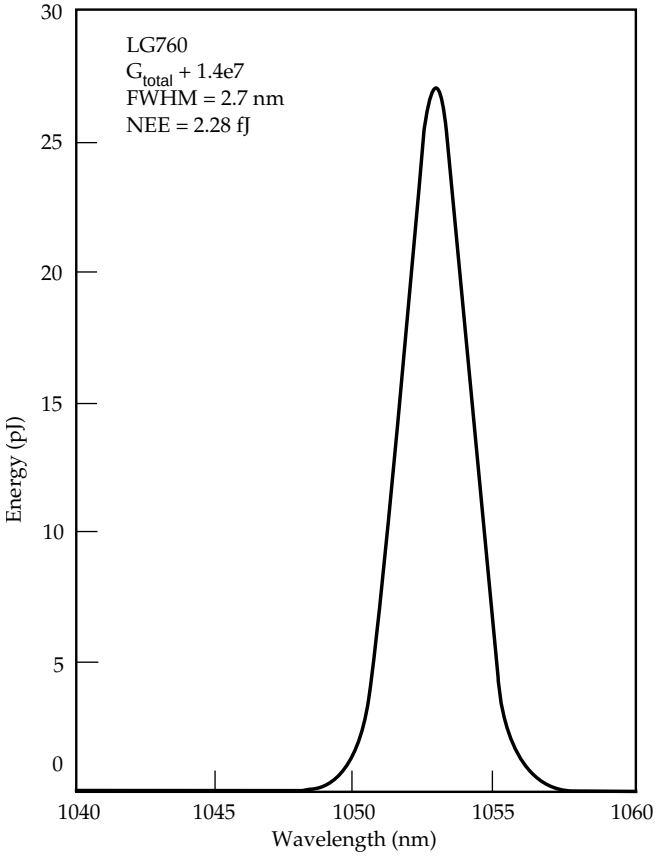

FIGURE 17. Quantum-limited noise spectrum for the regen with LG760 glass. (70-00-0298-0175pb01)

Gain Stability

Uniformity of target illumination, whether hohlraum or spherical target, flows down to a power-balance requirement for each of the 192 beamlines and, further, to the 48 PAMs. The current requirement for pulse-to-pulse fluctuation out of a preamplifier is 3% rms. This 3% value for the preamplifier output represents the total variation in output for one beamline of the OPG and must further be apportioned to the various subsystems, including the MOR, regenerative amplifier, and 4-pass amplifier. One of the early motivations for developing a diode-pumped regen was to reduce the pulse-to-pulse gain variation that is observed in flashlamp-pumped amplifiers.

To understand the source of fluctuations, we performed a simple differential analysis and then measured the individual contributors. The variation in output energy from the regen ΔE_{out} can be written as

$$\frac{\Delta E_{out}}{E_{out}} = \frac{\Delta E_s}{E_s} + \frac{\Delta T_s}{T_s} + \frac{k\Delta T_c}{T_c} + 2k(\Delta g_1 + \Delta g_2) \quad , \tag{13}$$

where T_s and T_c are the seed and cavity transmission, respectively, E_s is the input pulse energy from the MOR, k is the number of round trips, and g_1 and g_2 are the single-pass exponential gains of the diode-pumped amplifiers. These individual contributions to the overall variation in output energy of the regen can be grouped into high- and low-bandwidth effects. Low-bandwidth contributions include mechanical drift in optical mounts, mechanical vibrations that cause fluctuations in the polarization of the light emerging from

TABLE 2. Summary of regenerative amplifier performance.

Laser characteristic	NIF specification	Measured performance
1. Maximum output energy	—-	22 mJ
2. Required energy	10 mJ	10 mJ
3. Input energy	500 pJ	180 pJ
4. Total gain	2×10^7	5.5×10^7
5. Round trips	13–15	15
6. Cavity length (s)	—	30.5 ns
7. Cavity length (cm)	—	458 cm
8. Cavity configuration	—	linear, TEM_{00}
9. Cavity stability	—	$g^2 = 0.019$
10. Far-field beam profile	1.5 × D.L.	1.1 × D. L.
11. Near-field spatial amplitude modulation	<5%[a]	<1%
12. Pointing stability	<35 μrad[a]	<12 μrad
13. Gain stability	<0.03[a]	<0.014
14. Pulse repetition rate	1 Hz	1 Hz
15. Wavelength	1053 nm	1052.9 nm
16. Diode-pumped amplifiers	2	2
17. Diode driver current	—	92 A/head
18. Total electrical power to diodes	—	18.4 kW
19. Pump pulse length	—	350 μs
20. Total pump energy (optical)	—	2.1 J[b]
21. Total pump power at rods	—	6 kW[b]
22. Amplifier glass	—	LG760
23. Rod dimensions	—	5 mm (diam) × 50 mm
24. Stimulated emission cross section	—	4.67×10^{-20}
25. Saturation fluence	—	3.99 J/cm^2
26. Nd^{3+} doping	—	1%
27. Gain/pass/head	—	1.5[c]
28. Optical stored energy in rods	—	526 mJ[b]
29. Mode size in rod ($1/e^2$ radius), w_0	—	0.083 cm
30. Effective mode area/rod $A_{mode} = \pi w_0^2/2$	—	1.08×10^{-2}
31. Fill factor = A_{mode}/A_{rod}	—	0.055
32. Stored energy in mode	—	35 mJ[b]
33. Maximum extraction efficiency	—	0.62
34. Extraction efficiency at 10 mJ	—	0.29
35. Fraction of total stored energy extracted	—	1.9×10^{-2}
36. Optical effic. of regen = energy out/pump power	—	4.76×10^{-3}
37. Total wall-plug efficiency	—	1.55×10^{-3}
38. Square-pulse distortion (SPD) at 10-mJ output	1.2	1.17[d]
39. SPD at maximum output energy	—	—
40. Prepulse contrast ratio	10^5–10^6	4.8×10^5
41. Energy signal-to-noise ratio for 500-pJ input	10^4	3.56×10^4

[a]Specifications for the OPG. The flowdown has not yet been done for the regenerative amplifier.
[b]Combined value for both amplifiers.
[c]Average value of the two amplifiers .
[d]Achieved with recent upgrade to current design using single-diode head.

the single-mode fiber, and thermal drift in the temperature of the pump-diodes, causing a shift in the diode emission wavelength. We have solved most of these causes of slow drift of the regen output energy. For example, variations in diode temperature have been reduced by working with the manufacturer to improve heat sinking in the diode package, and by using a Nd:doped glass with a broader absorption spectrum that is less sensitive to the small changes in the diode wavelength. Higher-bandwidth contributions to gain fluctuations in Eq. (13) include pulse-to-pulse variations in the diode-driver current or voltage, and frequency chirp of the diode-emission frequency during the diode current pulse.

To identify sources of faster, pulse-to-pulse variations in the regen energy, we set up diagnostics to measure changes in those parameters that affect, or are related to, the gain in the rod amplifiers. In one experiment, we determined that the diode-current spontaneous emission from the rods, along with the regen output energy, all correlated on a shot-to-shot basis with small fluctuations in the voltage gate that controls the diode current. Figure 18 is a histogram showing the variation in regen output energy for 3000 shots. The solid line is a Gaussian fit to the data that yields a value of 1.4% for the rms variation of the output energy. This value is well within the 3% total variation for the preamplifier, but it does not allow much margin for variation in gain of the larger 4-pass amplifier. We are currently investigating ways to actively control the output energy of the regen to reduce energy fluctuations to less than 1% rms using high-bandwidth, feed-forward and feedback techniques.

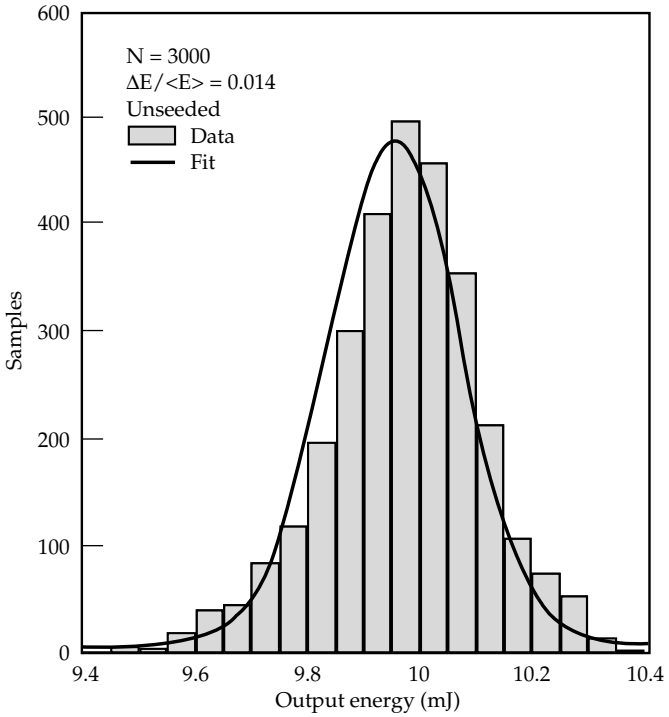

FIGURE 18. Histogram of the shot-to-shot variation in regen output energy. (70-00-0298-0176pb01)

Summary of Regenerative Amplifier Performance

Table 2 is a summary of the measured performance and operating conditions for the current regen prototype. For comparison, we include the specifications derived from a flowdown of the entire laser system. In all cases, the current design meets or surpasses the NIF performance specifications.

Conclusions

The diode-pumped regenerative amplifier is the highest-gain laser system in the NIF laser chain. It acts as a high-fidelity preamplifier to boost the output pulses from the MOR to an energy level for injection into the large laser power amplifiers that form the rest of a NIF laser chain. Our current design meets or surpasses all of the performance specifications derived from a flowdown of the entire laser system. Our principal activity in the near future will be to combine this prototype regen with the completed 4-pass amplifier and MOR in an integrated OPG testbed, and to assemble a similar regenerative amplifier in the first PAM prototype. The OPG testbed will be operated for the next year as a facility for demonstrating all performance requirements for the NIF OPG system.

Notes and References

1. J. Davin, *SSDR 1.3.1, Optical Pulse Generation Subsystem*, Lawrence Livermore National Laboratory, Livermore, CA, NIF-0000058-02, WBS 1.3.1 (1996).
2. *National Ignition Facility Conceptual Design Report*, *Vol. 2*, Lawrence Livermore National Laboratory, Livermore, CA, UCRL-PROP-117093, Version 2 (1994).
3. B. M. Van Wonterghem, J. T. Salmon, and R. W. Wilcox, "Beamlet Pulse Generation and Wavefront Control System," *ICF Program Annual Report 1995*, Lawrence Livermore National Laboratory, Livermore, CA, UCRL-LR-105820-95, 42–51 (1995).
4. F. G. Patterson, M. D. Perry, and J. T. Hunt, "Design and Performance of a Multiterawatt, Subpicosecond Neodymium:Glass Laser," *J. Opt. Soc. Am. B* **8**, 2384 (1991).
5. J. K. Crane, M. Martinez, R. J. Beach, S. Mitchell, G. Pratt, and J. J. Christensen, "Ultra-Stable, Diode-Pumped Nd-Doped Glass Regenerative Amplifier for the National Ignition Facility (NIF)," Conference on Lasers and Electrooptics (CLEO), Anaheim, CA, May 1996.
6. R. Beach et. al., "Scalable Diode-End-Pumping Technology Applied to a 100-mJ Q-Switched Nd^{3+}:YLF Laser Oscillator," *Opt. Lett.* **18**, 1326 (1993).
7. R. Beach, "Scalable Diode Pumping for End-Pumped Laser Systems," *Laser Tech. Briefs* **2**(1), 32–36 (1994).
8. This equation appears in many forms in most laser texts and is derived from the classical coupled atom-field equations. The time-integrated version of Eq. (9) is commonly called the Frantz–Nodvik equation. The particular form shown here can be found in A. E. Siegman, *Lasers* (University Science Books, Mill Valley CA, 1986), ch. 10.
9. R. Page and G. Wilke (private communication).
10. A. Yariv, *Quantum Electronics*, 2nd ed. (J. Wiley, New York, 1975).